ACS central science

Research Article

http://pubs.acs.org/journal/acscii

Catalytic Methane Monofunctionalization by an Electrogenerated High-Valent Pd Intermediate

Matthew E. O'Reilly, R. Soyoung Kim, Seokjoon Oh, and Yogesh Surendranath*

Department of Chemistry, Massachusetts Institute of Technology, Cambridge, Massachusetts 02139, United States

Supporting Information

ABSTRACT: Electrophilic high-valent metal ions are potent intermediates for the catalytic functionalization of methane, but in many cases, their high redox potentials make these intermediates difficult or impossible to access using mild stoichiometric oxidants derived from O_2. Herein, we establish electrochemical oxidation as a versatile new strategy for accessing high-valent methane monofunctionalization catalysts. We provide evidence for the electrochemical oxidation of simple $PdSO_4$ in concentrated sulfuric acid electrolytes to generate a putative $Pd_2^{III,III}$ species in an all-oxidic ligand field. This electrogenerated high-valent Pd complex rapidly activates methane with a low barrier of 25.9 (±2.6) kcal/mol, generating methanol precursors methyl bisulfate (CH_3OSO_3H) and methanesulfonic acid (CH_3SO_3H) via concurrent faradaic and nonfaradaic reaction pathways. This work enables new electrochemical approaches for promoting rapid methane monofunctionalization.

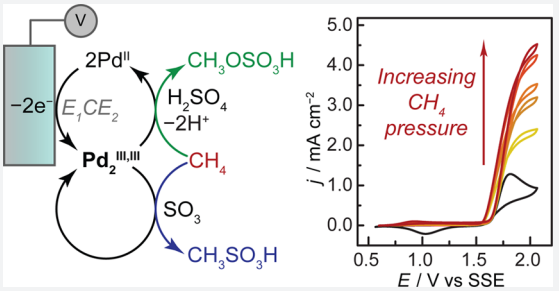

INTRODUCTION

Methane is an abundant, low-cost, carbon-based feedstock, but its chemical inertness and propensity for uncontrolled oxidation impedes its widespread utilization as a precursor to liquid fuels and commodity chemicals.[1−4] Existing technologies for the conversion of methane to liquid products proceed via a two-step indirect route that involves a high-temperature, capital-intensive process.[5] An alternative to this scenario is the use of homogeneous catalysts that employ transition metal and main group ions to activate the localized, low-energy filled orbitals within the C−H bonds of methane at milder temperatures.[6] In concentrated CF_3CO_2H and H_2SO_4 media, electrophilic ions mediate the two-electron oxidation of methane to methyl esters, which are protected from overoxidation by the electron-withdrawing effect of CF_3CO_2- and HSO_4- groups.[7] These methyl esters can be subsequently hydrolyzed to produce methanol. In these schemes, catalytic methane functionalization proceeds via two-electron redox cycling of the metal center. Apart from Pt-based catalysts that are known to activate the methane C−H bond in the low-valent Pt(II) state,[8−11] most catalysts activate methane in their high-valent form and generate the methanol product following reductive elimination to a lower valent species (Figure 1, left).[12,13] Irrespective of the mechanistic details, the two-electron redox potential of the metal center crudely approximates the driving force for oxidative methane functionalization (Figure 1, right, top arrow), and, invoking a linear free-energy correlation, metal ions with higher redox potentials are expected to functionalize methane more rapidly. Herein lies a central challenge for catalyst design: increasing the redox potential of the metal center accelerates methane functionalization[14] but simultaneously impedes reoxidation by the stoichiometric oxidant in the system (Figure 1, right, bottom arrow). As O_2 is the only viable terminal oxidant for large-scale methane functionalization, the redox potential of the metal catalyst cannot significantly exceed the O_2/H_2O redox potential, E° = 1.23 V. This constraint relegates metal centers that possess two-electron redox potentials positive of the O_2/H_2O couple, such as Tl^{III}, Pb^{IV},[15] and Au^{III},[16] to principally stoichiometric methane functionalization reactivity. Additionally, as O_2 is too sluggish and unselective to be used directly, the SO_3/SO_2 couple is commonly employed.[13] This oxidant is attractive because it can be regenerated via aerobic combustion over a

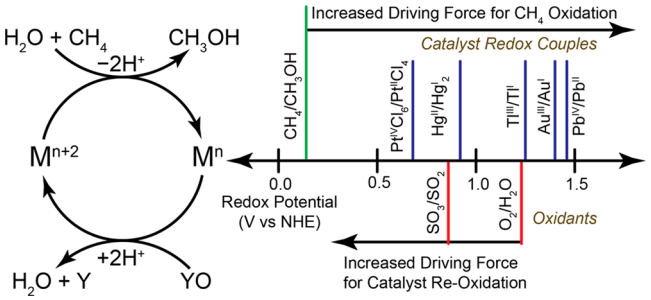

Figure 1. Redox potentials of methane oxidation catalysts. (Left) Simplified catalytic cycle for electrophilic methane oxidation using stoichiometric oxidant YO. (Right) Estimated redox potentials of electrophilic methane functionalization catalysts/reagents[21] compared to the values for the CH_4/CH_3OH, O_2/H_2O, and SO_3/SO_2 redox couples. Derivation of SO_3/SO_2 and CH_4/CH_3OH redox potentials is detailed in Tables S14 and S15.

Received: July 30, 2017
Published: October 12, 2017

DOI: 10.1021/acscentsci.7b00342
ACS Cent. Sci. 2017, 3, 1174−1179

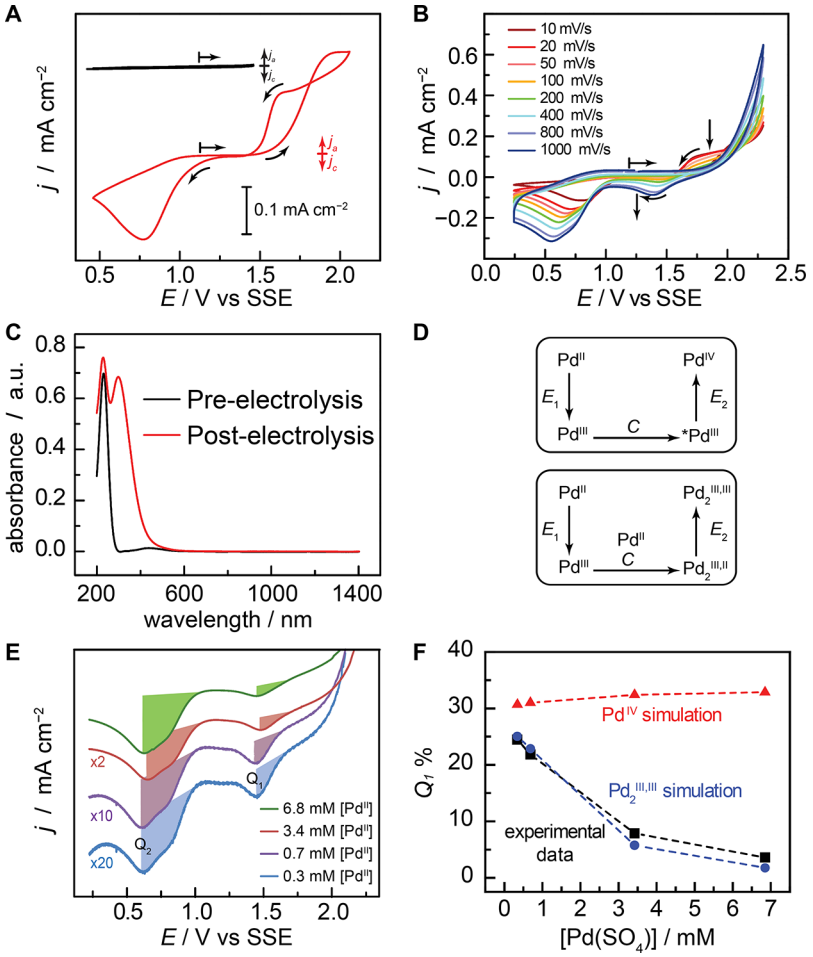

Figure 2. Evidence for an electrogenerated $Pd_2^{III,III}$ species. (A) CVs (50 mV/s scan rate) of $PdSO_4$ (~25 mM) in concentrated H_2SO_4. Arrows indicate potential of scan initiation and direction of scan. (B) Varying scan rate CVs of $PdSO_4$ (~24 mM) in concentrated H_2SO_4. Arrows indicate direction of scan and progression of waves at 1.41 and 1.75 V with increasing scan rate. (C) UV−vis spectra of $PdSO_4$ before (black) and after (red) electrolysis in concentrated H_2SO_4. (D) Proposed mononuclear and binuclear E_1CE_2 mechanisms. (E) Return scans of CVs (200 mV/s scan rate) recorded in four concentrations of $PdSO_4$ depicting the integrated charges, Q_1 and Q_2, of the back-reduction waves. (F) Simulated (red and blue) and experimental (black) percent integrated charge (Q_1 %) in the first back-reduction wave at $E_{p,c}$ = 1.41 V vs the concentration of $PdSO_4$. Dotted lines serve as guides to the eye.

V_2O_5 catalyst,[17] but the SO_3/SO_2 couple possesses an even lower redox potential, E° = 0.86 V (Tables S14 and S15), further reducing the driving force for catalyst reoxidation. This low driving force, combined with the kinetic sluggishness of S−O bond cleavage,[18,19] makes catalyst reoxidation rate-limiting in nearly all methane functionalization cycles that employ SO_3.[18,20] Clearly, practical methane functionalization schemes require the development of alternative approaches that provide for rapid catalyst reoxidation with a tunable driving force.

In principle, electrochemical methods for regenerating electrophilic high-valent catalysts could overcome this central reoxidation challenge. By varying the electrode potential, the driving force for reoxidation can be systemically controlled to maintain a nonequilibrium population of highly reactive high-valent species, even if their redox potentials are more positive than that of viable terminal oxidants such as O_2 and SO_3. By decoupling the metal redox potential from that of the terminal chemical oxidant (e.g., O_2), we envisioned that electrochemical methods can access high potential metal ions that would be capable of functionalizing methane at exceptional rates. Thus, continuous electrogeneration of these high-valent species in a concentrated acid medium could, in principle, enable new catalytic and electrocatalytic cycles for methane functionalization. The electrons extracted to maintain this pool of high-valent ions could be used to drive the reduction of O_2 to water at a separate electrode, allowing for continuous electrochemical methane functionalization. Previous efforts toward this goal were hampered by significant overoxidation on heterogeneous electrocatalysts, leading to <5% methanol selectivity on nickel oxide based systems.[22,23] In addition, the development of molecular electrocatalysts was impeded by the sluggish interfacial electron transfer kinetics typical of Pt-group ions.[24−26] The latter prevented direct electrochemical reoxidation on a timescale commensurate with methane functionalization.[27] Herein, we establish an electrochemical strategy for selective catalytic methane functionalization that employs electro-oxidation of $Pd^{II}SO_4$ in concentrated sulfuric acid to generate a putative $Pd_2^{III,III}$ intermediate. This species rapidly reacts with methane to generate precursors to methanol—CH_3OSO_3H and CH_3SO_3H—via concurrent electrocatalytic and nonfaradaic pathways, respectively.

DOI: 10.1021/acscentsci.7b00342
ACS Cent. Sci. 2017, 3, 1174−1179

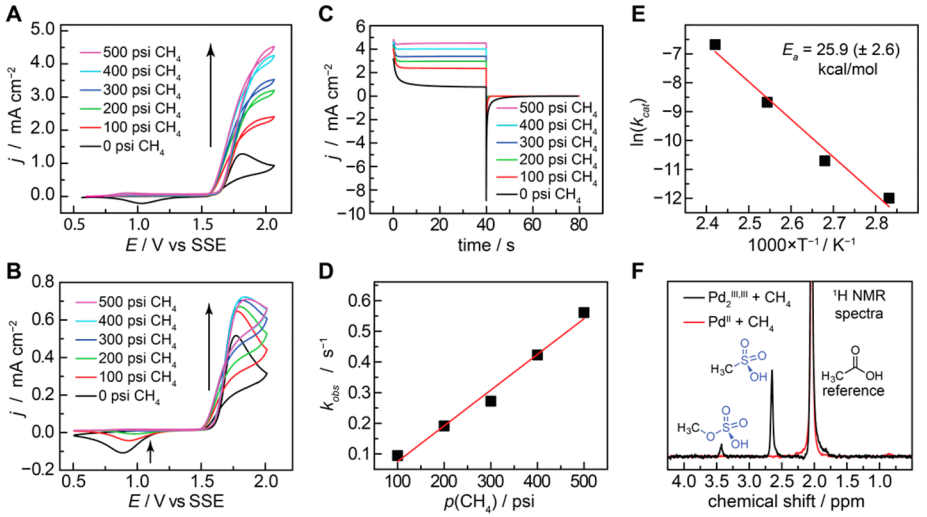

Figure 3. Methane functionalization by an electrogenerated $Pd_2^{III,III}$ species. CVs (20 mV/s scan rate) of $PdSO_4$ (~23 mM) in concentrated H_2SO_4 recorded at 140 °C (A) and 100 °C (B) with varying CH_4 pressure. (C) Double potential step chronoamperometry of $PdSO_4$ (~23 mM) in concentrated H_2SO_4 recorded at 140 °C with varying CH_4 pressure and step potentials of 2.0 V followed by 0.50 V. (D) Plot of k_{obs} vs CH_4 pressure at 140 °C. (E) Arrhenius plot of electrochemical methane oxidation rate constants, k_{cat} (psi^{-1} s^{-1}), between 80 and 140 °C. (F) ^1H NMR of the reaction mixture after treating a 4.2 mM $Pd_2^{III,III}$ (black) and 8.4 mM Pd^{II} (red) solution in 20% SO_3/H_2SO_4 with 500 psi of CH_4 at 100 °C for 20 min.

RESULTS AND DISCUSSION

Shown in Figure 2A is the cyclic voltammogram (CV) of $PdSO_4$ in concentrated, 95–98%, sulfuric acid electrolyte. Autoionization of the sulfuric acid removes the need for added electrolytes.[28] Fluorine-doped tin oxide (FTO) coated glass slides[29] served as corrosion-resistant working electrodes (Figure S1) under these conditions (see Materials and Methods). Background double layer charging current is observed between 0.42 and 1.46 V (Figure 2A, black; all potentials are reported vs the Ag_2SO_4/Ag (SSE) electrode[30−32]), whereas scanning to more positive potentials (Figure 2A, red) reveals an oxidative wave at $E_{p,a}$ = 1.96 V prior to solvent oxidation beyond 2.40 V. On the return scan, there is a pronounced hysteresis in the CV, with the forward and backward traces crossing at 1.75 V. Scanning into this oxidative wave is both necessary and sufficient to generate a broad reduction wave at 0.76 V on the cathodic scan. The hysteretic crossing of the forward and reverse CV traces is diagnostic[33] of an overall two-electron oxidation sequence that proceeds via an initial electron transfer step (E_1), a chemical reaction step (C), and a subsequent second electron transfer step (E_2) that occurs at a lower redox potential than the initial oxidation process. Together, these steps are denoted as an E_1CE_2 process.[33] The hysteretic behavior arises from the large inversion in redox potentials between the E_1 and E_2 steps; during the forward sweep, the E_1 and C steps form an intermediate that is easier to oxidize than the starting material, giving rise to additional current on the reverse trace. Although, in general, an E_1CE_2 mechanism can give rise to a disproportionation reaction following the C step, a high rate of disproportionation serves to eliminate the hysteretic behavior[33] (Figure S8), indicating that its role in the Pd oxidation sequence is minimal. The high-valent product of the E_1CE_2 sequence is then back-reduced to Pd^{II} in the broad wave at 0.76 V. CV data collected at varying scan rates (Figure 2B) further support an E_1CE_2 oxidation mechanism. At scan rates greater than 200 mV/s, we observe another cathodic wave at $E_{p,c}$ = 1.41 V, consistent with back-reduction of the mono-oxidized species, the reverse of E_1, occurring prior to the C step. Concomitantly, the hysteretic behavior centered at 1.75 V disappears at faster scan rates, consistent with this back-reduction beginning to outcompete the C step. Together the data establish that Pd^{II} solutions in concentrated sulfuric acid electrolyte undergo a two-electron oxidation via an E_1CE_2 sequence to generate a high-valent Pd species.

Spectroscopic data provide insight into the electronic structure of the electrogenerated species. The high-valent Pd species was generated by preparative bulk-electrolysis and displays a strong UV–vis absorption band (ε = 2.0 × 10^4 M^{-1} cm^{-1}; Figure S4B) centered at 300 nm (Figure 2C, red) that is absent in the Pd^{II} spectrum (Figure 2C, black). In situ UV–vis spectroelectrochemistry (Figure S3) reveals that this 300 nm band arises as a direct result of polarization beyond the oxidative wave. Notably, the high-valent species displays no detectable absorption bands at lower energies out to 1400 nm. Mononuclear, dinuclear, and polynuclear Pd complexes with unpaired spins display strong absorption bands (ε = 0.4–5.0 × 10^3 M^{-1} cm^{-1}) between 500 and 1000 nm;[34,35] thus the spectroscopic data obtained here suggest that the product generated via electro-oxidation is a ground-state singlet species. This postulate is supported by Evans method magnetic susceptibility measurements (Figure S5), which reveal that electro-oxidation generates a diamagnetic species at room temperature. Together, the spectroscopic data are consistent with either a mononuclear Pd^{IV} or a dinuclear $Pd_2^{III,III}$ complex. Both of these species can be formed via E_1CE_2 mechanisms that are depicted in Figure 2D and abbreviated as $Pd^{II}/Pd^{III}//{}^*Pd^{III}/Pd^{IV}$ or $Pd^{II}/Pd^{III}//Pd_2^{III,II}/Pd_2^{III,III}$, where / and // denote E and C steps, respectively.

To distinguish between the foregoing mechanistic possibilities, we collected CV data at four Pd^{II} concentrations ranging from 0.34 to 6.8 mM (Figure 2E). The magnitude of the back-reduction wave at ~1.4 V serves as a measure of the concentration of Pd^{III} at the electrode after scanning through the oxidative wave. We compared this result to the magnitude of the broad wave at ~0.75 V, a measure of the concentration of the two-electron oxidized product, $Pd_2^{III,III}$ or Pd^{IV}, generated

DOI: 10.1021/acscentsci.7b00342
ACS Cent. Sci. 2017, 3, 1174–1179

at the electrode. As the Pd^{II} concentration increases, the magnitude of the wave at ~1.4 V decreases relative to the magnitude of the wave at ~0.75 V, indicating that the rate of the C step is enhanced by increasing [Pd^{II}]. The observed concentration dependence excludes a purely mononuclear E_1CE_2 mechanism, $Pd^{II}/Pd^{III}//{}^*Pd^{III}/Pd^{IV}$. To further verify the mechanism, we simulated cyclic voltammograms (see Supporting Information for full simulation details) for both mononuclear (Figure S6) and dinuclear (Figure S7) mechanisms and found that the experimental percentage of charge passed in reducing the Pd^{III} intermediate, Q_1 % = 100 × Q_1/(Q_1 + Q_2) (Figure 2F, black squares), matches closely with the simulated Q_1 % for the dinuclear mechanism (Figure 2F, blue circles) and is in stark contrast to the roughly concentration-independent behavior observed in simulations of the mononuclear mechanism (Figure 2F, red triangles). Although these simulations exclude more complex mechanisms that might involve transient surface adsorption or oligomeric intermediates, the formation of an oligomeric product is inconsistent with the spectroscopic data detailed above.[35] Together these results suggest that electro-oxidation of Pd^{II} proceeds via an E_1CE_2 mechanism involving a dinuclear C step to generate a putative $Pd_2^{III,III}$ species. We note that well-characterized $Pd_2^{III,III}$ complexes are known to be key intermediates in C−H functionalization catalysis,[36,37] and our data suggest that similar species may be electrogenerated under these conditions. However, we acknowledge that the data presented here would also be consistent with a mixed-valent $Pd_2^{II,IV}$ species, and investigations aimed at parsing between these valence tautomers and further characterizing the structure of the complex are currently ongoing.

The putative $Pd_2^{III,III}$ species formed via electro-oxidation is highly active for electrocatalytic methane functionalization at elevated temperatures. At 140 °C, the CV scan of $PdSO_4$ in concentrated H_2SO_4 (Figure 3A, black) is similar to that recorded at ambient temperature (Figure 2A, red). As in the room temperature CV, a hysteretic anodic peak is observed at $E_{p,a}$ = 1.82 V along with a broad reduction feature at $E_{p,c}$ = 1.03 V, indicating that the same E_1CE_2 mechanism to generate the putative $Pd_2^{III,III}$ species is operative at elevated temperatures. Upon charging the electrochemical cell with 100 psi of methane (Figure 3A, red), the anodic peak at 1.82 V transforms into a catalytic wave, the magnitude of which continues to rise with increasing methane pressure up to 500 psi (Figure 3A, violet). Consistent with electrocatalytic regeneration of the Pd^{II} via methane oxidation, the broad reduction peak at 1.03 V disappears completely in the presence of methane. Electrocatalytic methane oxidation is observed at lower temperatures as well. At 100 °C, increasing the methane pressure leads to a less pronounced rise in the anodic current beyond 1.5 V, but nonetheless leads to a diminution of the $Pd_2^{III,III}$ back-reduction peak (Figure 3B), indicating consumption of the high-valent species via methane oxidation. Notably, there is a decline in the magnitude of this back-reduction wave at temperatures as low as 80 °C (Figure S9), revealing the potency of the putative $Pd_2^{III,III}$ in carrying out methane oxidation catalysis.

To extract the rate constant for methane oxidation by the electrogenerated $Pd_2^{III,III}$ species, we collected chronoamperograms at 2.0 V, well beyond the 1.82 V anodic peak potential corresponding to formation of this species. At 140 °C, in the absence of methane (Figure 3C), a diffusion-limited decay of the anodic current is observed, whereas, in the presence of methane, steady-state electrocatalysis is observed with anodic currents that are invariant with time. The high electrochemical driving force for generating the putative $Pd_2^{III,III}$ and the time invariance of the chronoamperogram indicate that the current flow is limited, in this regime, by the activation-controlled rate of methane oxidation by the putative $Pd_2^{III,III}$ species. Under pure kinetic conditions, the following relationship holds:[38]

$$\frac{j_{[CH_4]}}{j_0} = \sqrt{\pi k_{obs}}\sqrt{t} \quad (1)$$

where t is time, $j_{[CH_4]}$ and j_0 are the current densities in the presence and absence of methane, respectively, and k_{obs} (s^{-1}) is the apparent rate constant for methane functionalization. Working curves were produced by plotting $j_{[CH_4]}/j_0$ vs $t^{1/2}$ (Figure S10 and S11), and linear regions of these plots, which correspond to activation-controlled kinetics, were used to extract k_{obs}. At 140 °C and 500 psi of methane, the turnover frequency of electrocatalytic methane oxidation is 2000 h^{-1}. Under identical conditions, $Pd^{II}(SO_4)$ catalyzes methane functionalization by itself, but with a turnover frequency of 0.4 h^{-1}, indicating that electrical polarization serves to *increase the rate of methane functionalization by 5000-fold* (Table S16). Indeed, the $Pd_2^{III,III}$ species functionalizes methane at rates >*20-fold faster* than state-of-the-art nonelectrochemical catalysts, K_2PtCl_4 and (2,2′-bipyrimidyl)$PtCl_2$,[9,39] which, at the same temperature and methane pressure, display turnover frequencies of 90 h^{-1} and 6 h^{-1} (Table S16) respectively in fuming sulfuric acid. These comparisons illustrate the power of electrical polarization to drive methane functionalization at extremely high rates while maintaining modest reaction temperatures that may be more amenable to process integration.

Concentration-dependent studies were used to further characterize the mechanism of methane functionalization. We observed a first-order dependence of k_{obs} on methane concentration (Figure 3D) that indicates a bimolecular reaction between the putative $Pd_2^{III,III}$ intermediate and methane prior to or during the rate-limiting step of catalysis. Slopes of these plots were used to extract bimolecular rate constants, k_{cat} (psi^{-1} s^{-1}), for methane electro-oxidation, and an Arrhenius plot of these values over the 80−140 °C temperature range provides an activation energy barrier of E_a = 25.9 (±2.6) kcal/mol (Figure 3E), which is consistent with the very high rate of catalysis and is among the lowest experimental values reported for oxidative methane functionalization (Table S17). Additionally, the foregoing discussion highlights the power of electrochemical methods for extracting the kinetics of methane functionalization, data that have thus far been difficult to obtain using stoichiometric oxidants.

To identify the products of methane functionalization, we subjected a 4.2 mM solution of $Pd_2^{III,III}$ in 20% SO_3/H_2SO_4, generated via preparative bulk electrolysis of Pd^{II}, to 500 psi of methane at 100 °C for 20 min. The added SO_3 suppressed the slow thermal decay of the $Pd_2^{III,III}$ species via water oxidation. UV−vis spectroscopy of the sample following the reaction (Figure S12) establishes the quantitative regeneration of Pd^{II} over this time period, and the ^1H NMR spectrum of the reaction mixture reveals the formation of 0.5 (±0.1) equivalents of CH_3OSO_3H, indicating that, under these reaction conditions, all of the oxidizing equivalents in the $Pd_2^{III,III}$ species go toward the two-electron oxidation of methane to a methanol derivative (Figure 3F). Because methane oxidation is a two-

DOI: 10.1021/acscentsci.7b00342
ACS Cent. Sci. 2017, 3, 1174−1179

electron process, this reaction stoichiometry provides further evidence in support of an average Pd oxidation state of 3+ in the electrogenerated species. Remarkably, CH_3OSO_3H is not the only product of the reaction; we also observe 34 (±12) mM CH_3SO_3H, the product of the net redox-neutral insertion of SO_3 into the C−H bond of methane.[40] The same reaction, conducted in the presence of Pd^{II}, displays no methane functionalization products at this temperature, indicating that the electrogenerated $Pd_2^{III,III}$ species is uniquely responsible for both carrying out oxidative methane functionalization to generate CH_3OSO_3H and catalyzing nonfaradaic methane sulfonation to generate CH_3SO_3H. In further support of this conclusion, we do not observe additional CH_3SO_3H if the reaction time is extended beyond the timescale of $Pd_2^{III,III}$ consumption (Table S12). Given the ∼7-fold excess of CH_3SO_3H relative to CH_3OSO_3H that we observe under these conditions, these data indicate that the $Pd_2^{III,III}$ catalyzes methane sulfonation at rates significantly higher than the rate of electrocatalytic methane oxidation measured electrochemically. Since CH_3SO_3H is known to convert to CH_3OSO_3H upon thermolysis, this sulfonation reaction pathway would not compromise net reaction selectivity in a well-engineered system.[41,42]

In an optimally engineered electrochemical cell, continuous electroregeneration of the putative $Pd_2^{III,III}$ species would permit methane sulfonation and electro-oxidation to proceed indefinitely. Bulk electrolysis of Pd^{II} at 70 °C in a stirred 20% SO_3/H_2SO_4 electrolyte in the presence of 500 psi of methane led to a sustained catalytic current of 0.65 mA/cm^2 that is unchanged over the course of 5 h (Figure S14). A relatively low temperature was chosen for this measurement to minimize convolution from a slow background reaction with Pd^{II} (see Supporting Information for details). ^{1}H NMR spectroscopic analysis of the reaction mixture following electrolysis reveals the formation of both CH_3OSO_3H and CH_3SO_3H in a ratio of ∼1:14. Remarkably, owing to simultaneous faradaic and nonfaradaic methane functionalization reactions, ∼3.4 molecules of methane are functionalized per electron passed, with a low ∼7% of the product subject to overoxidation to CO_2. The low electron stoichiometry of methane functionalization serves to improve the electrical energy efficiency of this system while maintaining extremely high rates of catalysis.

CONCLUDING REMARKS

These results demonstrate a simple strategy for selective methane monofunctionalization at modest temperatures via electrochemical oxidation of simple Pd^{II} salts in concentrated sulfuric acid solutions. Together, the data are consistent with a mechanistic model (Figure 4) for electroinduced methane functionalization catalysis under these conditions. Electrochemical oxidation of Pd^{II} proceeds via an E_1CE_2 sequence to generate a putative $Pd_2^{III,III}$ intermediate, which rapidly functionalizes methane via concurrent faradaic and nonfaradaic pathways to generate CH_3OSO_3H and CH_3SO_3H, respectively. Both CH_3OSO_3H and CH_3SO_3H can be thermally and hydrolytically converted to methanol,[41,42] providing, in net, a viable electropromoted pathway for selective methane functionalization. The power of electrochemistry to generate and maintain a nonequilibrium population of highly reactive high-valent metal species opens the possibility of using this methodology to access a wider range of metal ion catalysts for the functionalization of diverse chemically inert substrates. As we demonstrate here, the electrogenerated high-valent species

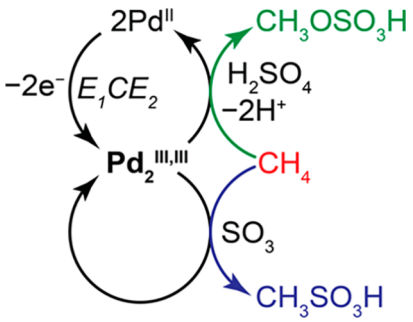

Figure 4. Proposed mechanism for electrochemical methane functionalization by a putative $Pd_2^{III,III}$ intermediate. Green and blue arrows indicate faradaic and nonfaradaic reaction pathways, respectively.

can carry out both faradaic and nonfaradaic reactions, reducing the electron stoichiometry of the process and enhancing its electrical efficiency. Combining this methodology with established methods for carrying out oxygen reduction catalysis provides a new electrochemical strategy for accelerating kinetically challenging aerobic C−H bond functionalization reactions.

ASSOCIATED CONTENT

Supporting Information

The Supporting Information is available free of charge on the ACS Publications website at DOI: 10.1021/acscentsci.7b00342.

Materials and methods, simulations of electrochemical data, additional spectroscopic data, and original data for rate measurements (PDF)

AUTHOR INFORMATION

Corresponding Author

*E-mail: yogi@mit.edu.

ORCID

Yogesh Surendranath: 0000-0003-1016-3420

Notes

The authors declare no competing financial interest.

ACKNOWLEDGMENTS

The authors gratefully acknowledge Prof. Cyrille Costentin and Jo Melville for many helpful discussions. This work was supported by Eni S.p.A. through the MIT Energy Initiative and by the MIT Department of Chemistry through junior faculty funds for Y.S.

REFERENCES

(1) Olah, G. A.; Goeppert, A.; Prakash, G. K. S. *Beyond oil and gas: the methanol economy*; Wiley-VCH: Weinheim, Germany, 2006.

(2) Wolf, E. E. *Methane conversion by oxidative processes: fundamental and engineering aspects*; Van Nostrand Reinhold: New York, 1992.

(3) Alvarez-Galvan, M. C.; Mota, N.; Ojeda, M.; Rojas, S.; Navarro, R. M.; Fierro, J. L. G. Direct methane conversion routes to chemicals and fuels. *Catal. Today* **2011**, *171*, 15−23.

(4) Curry-Hyde, H. E.; Howe, R. F. *Natural Gas Conversion II: proceedings of the Third Natural Gas Conversion Symposium*; Elsevier: Amsterdam, 1994; Vol. *81*.

(5) Rostrup-Nielsen, J.; Christiansen, L. J. *Concepts in syngas manufacture*; Catalytic Science Series; Imperial College Press: London, 2011.

(6) Labinger, J. A.; Bercaw, J. E. Understanding and exploiting C-H bond activation. *Nature* **2002**, *417*, 507−514.

DOI: 10.1021/acscentsci.7b00342
ACS Cent. Sci. 2017, 3, 1174−1179

(7) Ahlquist, M.; Nielsen, R. J.; Periana, R. A.; Goddard, W. A., III Product Protection, the Key to Developing High Performance Methane Selective Oxidation Catalysts. *J. Am. Chem. Soc.* **2009**, *131*, 17110−17115.
(8) Kushch, L. A.; Lavrushko, V. V.; Misharin, Y. S.; Moravsky, A. P.; Shilov, A. E. Kinetics and mechanism of methane oxidation in aqueous solutions of platinum complexes. Direct evidence for a methylplatinum intermediate. *New J. Chem.* **1983**, *7*, 729.
(9) Periana, R. A.; Taube, D. J.; Gamble, S.; Taube, H.; Satoh, T.; Fujii, H. Platinum catalysts for the high-yield oxidation of methane to a methanol derivative. *Science* **1998**, *280*, 560−564.
(10) Stahl, S. S.; Labinger, J. A.; Bercaw, J. E. Homogeneous Oxidation of Alkanes by Electrophilic Late Transition Metals. *Angew. Chem., Int. Ed.* **1998**, *37*, 2180−2192.
(11) While Pd(II) also activates methane, it is thought to undergo functionalization at the Pd(II) oxidation state, going through a Pd(II)/Pd(0) cycle. Therefore, Pd(II) in this catalytic sequence is the high-valent form. Please refer to ref 12 and 13 for more information.
(12) Hashiguchi, B. G.; Hövelmann, C. H.; Bischof, S. M.; Lokare, K. S.; Leung, C. H.; Periana, R. A. Methane-to-Methanol Conversion. In *Encyclopedia of Inorganic and Bioinorganic Chemistry*; John Wiley & Sons: New York, 2011.
(13) Gunsalus, N. J.; Koppaka, A.; Park, S. H.; Bischof, S. M.; Hashiguchi, B. G.; Periana, R. A. Homogeneous Functionalization of Methane. *Chem. Rev.* **2017**, *117*, 8521−8573.
(14) Among main group d^{10} ions (Hg(II), Tl(III), and Pb(IV)), the rate of methane functionalization has been found to correlate with the corresponding two-electron redox potential of the metal center. Please refer to ref 15 for more information.
(15) Hashiguchi, B. G.; Konnick, M. M.; Bischof, S. M.; Gustafson, S. J.; Devarajan, D.; Gunsalus, N.; Ess, D. H.; Periana, R. A. Main-Group Compounds Selectively Oxidize Mixtures of Methane, Ethane, and Propane to Alcohol Esters. *Science* **2014**, *343*, 1232−1237.
(16) Jones, C. J.; Taube, D.; Ziatdinov, V. R.; Periana, R. A.; Nielsen, R. J.; Oxgaard, J.; Goddard, W. A. Selective oxidation of methane to methanol catalyzed, with C-H activation, by homogeneous, cationic gold. *Angew. Chem., Int. Ed.* **2004**, *43*, 4626−4629.
(17) Müller, H. Sulfuric Acid and Sulfur Trioxide. In *Ullmann's Encyclopedia of Industrial Chemistry*; Wiley-VCH: Weinheim, 2000.
(18) Fuller, J. T.; Butler, S.; Devarajan, D.; Jacobs, A.; Hashiguchi, B. G.; Konnick, M. M.; Goddard, W. A.; Gonzales, J.; Periana, R. A.; Ess, D. H. Catalytic Mechanism and Efficiency of Methane Oxidation by Hg(II) in Sulfuric Acid and Comparison to Radical Initiated Conditions. *ACS Catal.* **2016**, *6*, 4312−4322.
(19) Hristov, I. H.; Ziegler, T. The Possible Role of SO_3 as an Oxidizing Agent in Methane Functionalization by the Catalytica Process. A Density Functional Theory Study. *Organometallics* **2003**, *22*, 1668−1674.
(20) Mironov, O. A.; Bischof, S. M.; Konnick, M. M.; Hashiguchi, B. G.; Ziatdinov, V. R.; Goddard, W. A.; Ahlquist, M.; Periana, R. A. Using Reduced Catalysts for Oxidation Reactions: Mechanistic Studies of the ″Periana-Catalytica″ System for CH_4 Oxidation. *J. Am. Chem. Soc.* **2013**, *135*, 14644−14658.
(21) Haynes, W. M.; *CRC Handbook of Chemistry and Physics*, 97th ed.; CRC Press: Boca Raton, FL, 2016.
(22) Spinner, N.; Mustain, W. E. Electrochemical Methane Activation and Conversion to Oxygenates at Room Temperature. *J. Electrochem. Soc.* **2013**, *160*, F1275−F1281.
(23) Omasta, T. J.; Rigdon, W. A.; Lewis, C. A.; Stanis, R. J.; Liu, R.; Fan, C. Q.; Mustain, W. E. Two Pathways for Near Room Temperature Electrochemical Conversion of Methane to Methanol. *ECS Trans.* **2015**, *66*, 129−136.
(24) Lappin, G. *Redox Mechanisms in Inorganic Chemistry*; Ellis Horwood: New York, 1994; p 285.
(25) Jude, H.; Krause Bauer, J. A.; Connick, W. B. An outer-sphere two-electron platinum reagent. *J. Am. Chem. Soc.* **2003**, *125*, 3446−3447.
(26) Hubbard, A. T.; Anson, F. C. Study of Electrochemistry of Chloride and Bromide Complexes of Platinum(II) and -(IV) by Thin Layer Electrochemistry. *Anal. Chem.* **1966**, *38*, 1887−1893.
(27) Freund, M. S.; Labinger, J. A.; Lewis, N. S.; Bercaw, J. E. Electrocatalytic Functionalization of Alkanes Using Aqueous Platinum Salts. *J. Mol. Catal.* **1994**, *87*, L11−L15.
(28) Waddington, T. C. *Non-aqueous solvent systems*; Academic Press: New York, 1965.
(29) Polczynski, P.; Jurczakowski, R.; Grochala, W. Strong and Long-Lived Free-Radical Oxidizer Based on Silver(II). Mechanism of Ag(I) Electrooxidation in Concentrated H_2SO_4. *J. Phys. Chem. C* **2013**, *117*, 20689−20696.
(30) Arvía, A. J.; Carrozza, J. S. W. The electrolysis of fuming sulphuric acids. *Electrochim. Acta* **1966**, *11*, 1641−1649.
(31) Garrera, H. A.; Carrozza, J. S. W.; Arvía, A. J. Electrochemical study of fuming sulphuric acids—I. Kinetic parameters of the anodic and cathodic reactions on platinum electrodes. *Electrochim. Acta* **1968**, *13*, 771−780.
(32) Carrozza, J. S. W.; Garrera, H. A.; Arvía, A. J. Electrochemistry of fuming sulphuric acids—II. Current/voltage characteristics at a platinum rotating disk electrode. *Electrochim. Acta* **1969**, *14*, 205−216.
(33) Savéant, J. M. *Elements of molecular and biomolecular electrochemistry: an electrochemical approach to electron transfer chemistry*; Wiley-Interscience: Hoboken, NJ, 2006.
(34) Mirica, L. M.; Khusnutdinova, J. R. Structure and electronic properties of Pd(III) complexes. *Coord. Chem. Rev.* **2013**, *257*, 299−314.
(35) Campbell, M. G.; Powers, D. C.; Raynaud, J.; Graham, M. J.; Xie, P.; Lee, E.; Ritter, T. Synthesis and structure of solution-stable one-dimensional palladium wires. *Nat. Chem.* **2011**, *3*, 949−953.
(36) Powers, D. C.; Ritter, T. Bimetallic Pd(III) complexes in palladium-catalysed carbon−heteroatom bond formation. *Nat. Chem.* **2009**, *1*, 302−309.
(37) Powers, D. C.; Benitez, D.; Tkatchouk, E.; Goddard, W. A.; Ritter, T. Bimetallic Reductive Elimination from Dinuclear Pd(III) Complexes. *J. Am. Chem. Soc.* **2010**, *132*, 14092−14103.
(38) Bard, A. J.; Faulkner, L. R. *Electrochemical methods: fundamentals and applications*; Wiley: New York, 1980; pp 503−506.
(39) Zimmermann, T.; Soorholtz, M.; Bilke, M.; Schuth, F. Selective Methane Oxidation Catalyzed by Platinum Salts in Oleum at Turnover Frequencies of Large-Scale Industrial Processes. *J. Am. Chem. Soc.* **2016**, *138*, 12395−12400.
(40) Mukhopadhyay, S.; Bell, A. T. Direct Sulfonation of Methane to Methanesulfonic Acid with SO_2 Using Ca Salts as Promoters. *J. Am. Chem. Soc.* **2003**, *125*, 4406−4407.
(41) Mukhopadhyay, S.; Zerella, M.; Bell, A. T. A high-yield, liquid-phase approach for the partial oxidation of methane to methanol using SO_3 as the oxidant. *Adv. Synth. Catal.* **2005**, *347*, 1203−1206.
(42) Basickes, N.; Hogan, T. E.; Sen, A. Radical-Initiated Functionalization of Methane and Ethane in Fuming Sulfuric Acid. *J. Am. Chem. Soc.* **1996**, *118*, 13111−13112.

DOI: 10.1021/acscentsci.7b00342
ACS Cent. Sci. 2017, 3, 1174−1179